PHYSICAL REVIEW D **82,** 114512 (2010)

Preconditioning maximal center gauge with stout link smearing in $SU(3)$

Alan Ó Cais,[1,2,*] Waseem Kamleh,[1] Kurt Langfeld,[3] Ben Lasscock,[1] Derek Leinweber,[1] Peter Moran,[1] Andre Sternbeck,[1,4] and Lorenz von Smekal[1,5]

[1]*Special Research Center for the Subatomic Structure of Matter, School of Chemistry and Physics, University of Adelaide, SA 5005, Australia*

[2]*Cyprus Institute, Guy Ourisson Building, Athalassa Campus, P.O. Box 27456, 1645 Nicosia, Cyprus*

[3]*School of Maths and Stats, University of Plymouth, Plymouth, PL4 8AA, United Kingdom*

[4]*Institut für Theoretische Physik, Universität Regensburg, D-93040 Regensburg, Germany*

[5]*Institut für Kernphysik, Technische Universität Darmstadt, Schlossgartenstrasse 9, D-64289 Darmstadt, Germany*

(Received 2 July 2008; revised manuscript received 17 September 2010; published 22 December 2010)

Center vortices are studied in $SU(3)$ gauge theory using maximal center gauge (MCG) fixing. Stout link smearing and over-improved stout link smearing are used to construct a preconditioning gauge-field transformation which is applied to the original gauge field before fixing to MCG. We find that preconditioning successfully achieves higher maxima of the gauge functional used in MCG. We observe a reduction in the number of identified vortices when this preconditioning method is used, and also a reduction in the string tension as measured on the identified vortex matter.

DOI: 10.1103/PhysRevD.82.114512 PACS numbers: 12.38.Gc, 11.15.Ha, 12.38.Aw

I. INTRODUCTION

Despite more than 30 years of intense study, quark color confinement in hadron physics remains unexplained (for an overview see Ref. [1]). Within the framework of lattice gauge theory, a popular viewpoint has been that quark confinement is the result of a particular class of gauge-field configurations which dominate the QCD vacuum on large distance scales. Two potential candidates have been most commonly investigated: confinement by means of center vortices and confinement due to Abelian monopoles (for a critical discussion of both see Ref. [2]). To enhance these particular features, gauge fields can first be fixed to a suitable gauge, such as maximal Abelian gauge (MAG) [3] or maximal center gauge (MCG) [4]. Monopoles and center vortices are then defined by the projection of these gauge-fixed fields onto $U(1)^{N-1}$ or Z_N, respectively. Significant progress to date has occurred in $SU(2)$ using MAG and MCG, with original findings reproducing about 90% [5] and about 100% [6], respectively, of the non-Abelian string tension. Removing monopole [7–9] or center-vortex [9–14] degrees of freedom from $SU(2)$ lattice gauge fields appears to leave topologically trivial, nonconfining gauge fields that do not spontaneously break chiral symmetry.

The significance of the center of the gauge group is what connects possible candidates for this special class of configurations. As outlined for the case of Laplacian center gauge (LCG) in Ref. [15], *all* monopole world lines are embedded in two-dimensional vortex surfaces. These topological objects naturally occur together as local gauge defects. In MCG it has been observed computationally that over 90% of monopole currents are localized on center vortices [16,17]. Strongly correlated effects between the two have also been observed by means of studying monopoles after vortex removal and vice versa [18], as well as through the effect of their removal on the spectra of the overlap Dirac operator [9].

Again, all these advancements have been in $SU(2)$, and work in $SU(3)$ has not progressed to this level. While initial investigations were hopeful [19,20], subsequent results for MCG [21,22] had difficulty in reproducing the full non-Abelian string tension. Investigations using MAG were also discouraging [23]; however, subsequent analysis has observed good Abelian dominance [24] in full QCD (but with significant deviations reported in the same study for the quenched case). Earlier studies in $SU(2)$ using MCG reported that the center-projected configurations recovered the full string tension; however, further study into the ambiguities of the gauge-fixing procedure showed that this result is plagued by Gribov-copy effects [25–27]: methods which give higher values of the gauge-fixing functional produce smaller values for the vortex-induced string tension. We point out that when the Laplacian center gauge of Refs. [15,28] (which is free of Gribov ambiguities on the lattice) is used as the fixing method, the full $SU(3)$ [and $SU(2)$] string tension is recovered for the center-projected gauge fields but *only* in the continuum limit. However, unlike MCG vortices [29], the interpretation of LCG vortex matter is cumbersome in the same continuum limit [21,30].

In this paper we focus on the Gribov problem of the $SU(3)$ center-vortex picture of confinement using the MCG fixing method. The approach adopted here has analogies with those conducted in Refs. [5,24] in that multiple Gribov copies are created and, for every configuration, that with the highest value of the gauge functional is chosen. This is done in a manner where we apply the

*a.ocais@cyi.ac.cy

''smeared gauge-fixing'' method of Ref. [31] (originally introduced for Landau gauge) to MCG. That is, we create a gauge transformation that brings a smeared configuration to MCG and apply this transformation as a preconditioning gauge transformation to the unsmeared configuration before fixing this to MCG. As for Landau gauge, such gauge-fixed configurations are expected to reach higher values for the gauge functional than without preconditioning, which thus provides a convenient way to ameliorate the Gribov problem, even though it cannot be solved completely. We investigate the effect of this method on the features of the long-distance behavior of the static quark potential as evaluated on configurations where the vortices derived from MCG have been removed and on configurations composed purely of these vortices. In $SU(2)$, it has been shown that center-vortex removal specifically targets topological properties [9,12], so as well as using stout link smearing [32], we also employ over-improved stout link smearing [33] to attempt to exploit the link to topological structure [34].

II. METHODOLOGY

A. Identifying vortex matter

In the center-vortex picture of confinement the gauge fields are considered to be decomposed into a long-range field Z_μ carrying all the confining fluctuations and a short-range field V_μ containing nonconfining perturbations,

$$U_\mu(x) = Z_\mu(x)V_\mu(x). \tag{1}$$

Here $Z_\mu(x)$ is the center element which is closest, on the $SU(3)$ group manifold, to $U_\mu(x)$. A vortex is a configuration of the gauge potentials topologically characterized by nontrivial elements of Z_3 and is created by a singular gauge transformation. The nontrivial center element of the singular gauge transformation characterizing the vortex may be made to be distributed over many links of an encircling loop [due to the short-range effects of $V_\mu(x)$]. If we assume that by a gauge transformation the nontrivial center element can be concentrated on just one link, we can compress this *thick* vortex into a *thin* one. If we then project this gauge-transformed configuration onto its center elements, the projected vortices (P vortices) linking with the loop should then correspond to the thin vortex. It is for this reason that we adopt the use of gauge fixing to obtain the necessary gauge transformation. It is the choice of gauge that determines our method for finding the center vortices and, therefore, the connection between the P vortices and the thick center vortices present in the original configuration. The Gribov problem associated with any gauge-fixing approach together with the particular choice of gauge and the properties of the P vortices derived from this choice are what have polarized opinions in this area [15,21,25,35,36].

Here, we employ the MCG gauge-fixing algorithm as outlined in Ref. [21]. The gauge functional we chose to maximize [with respect to the gauge transformations $\Omega(x)$] in this algorithm is

$$V_U[\Omega] = \frac{1}{N_l}\sum_{x,\mu}\left[\frac{1}{3}\,\mathrm{tr}U^\Omega_\mu(x)\right]\left[\frac{1}{3}\,\mathrm{tr}U^\Omega_\mu(x)\right]^\dagger, \tag{2}$$

where N_l is the number of links on the lattice and $U^\Omega \equiv \Omega(x)U_\mu(x)\Omega^\dagger(x+\mu)$ is the gauge-transformed field.

After fixing the gauge, each link should be close to a center element of $SU(3)$ [on the $SU(3)$ group manifold], $Z^m = e^{i\phi^m}$, where $\phi^m = \frac{2\pi}{3}m$ with $m \in \{-1, 0, 1\}$. This is determined by using a polar decomposition for every link,

$$\tfrac{1}{3}\,\mathrm{tr}U^\Omega_\mu(x) = u_{x,\mu}e^{i\phi_{x,\mu}}, \tag{3}$$

where $\phi_{x,\mu}$ should be near (typically within 5% at a tolerance level of 10^{-9} for the MCG algorithm) some ϕ^m by construction of the gauge-fixing condition. We then perform the center projection by mapping

$$SU(3) \mapsto Z_3\colon\ U^\Omega_\mu(x) \mapsto Z_\mu(x) \quad \text{with} \quad Z_\mu(x) = e^{i\phi^m_{x,\mu}},$$

with the appropriate choice of $\phi^m_{x,\mu}$, $m \in \{-1, 0, 1\}$, as determined by the polar decomposition of the link.

To reveal the vortex matter we simply take a product of links around an elementary plaquette composed of the center-projected links. We say a vortex pierces the plaquette if this product is a nontrivial center element, and the plaquette is then a P *vortex*. We can remove these P vortices from the configuration by hand using $U'_\mu(x) = Z^\dagger_\mu(x)U^\Omega_\mu(x)$.

B. Smearing as a preconditioner

As said above, in the center-vortex picture of confinement, the center-projected links Z_μ are expected to carry all the long-range (confining) fluctuation of the gauge-field configuration. It would seem reasonable then to employ the use of smearing to smooth out the short-range fluctuations of U_μ and allow the gauge-fixing procedure described above to see more of the underlying long-range physics. In Ref. [31], the authors utilize this approach to create a preconditioning method that attempts to solve the Gribov problem for Landau gauge. We adopt the same method here in the case of center gauge, constructing a preconditioning gauge transformation for each gauge field that achieves higher maxima in the gauge-fixing procedure and thereby directly addresses the Gribov-copy issue.

First, we smear the gauge-field links U_μ using stout link smearing [32]. The smeared link is given by

$$\tilde{U}_\mu(x) = \exp(iQ_\mu(x))U_\mu(x), \tag{4}$$

with

$$Q_\mu(x) = \frac{i}{2}(\Omega^\dagger_\mu(x) - \Omega_\mu(x)) - \frac{i}{6}\,\mathrm{tr}(\Omega^\dagger_\mu(x) - \Omega_\mu(x)),$$
$$\Omega_\mu(x) = C_\mu(x)U^\dagger_\mu(x)$$

and

$$C_\mu(x) = \rho_{\rm sm} \sum \{1 \times 1 \text{ staples touching } U_\mu(x)\}.$$

We have chosen to use an isotropic four-dimensional constant $\rho_{\rm sm}$ in $C_\mu(x)$, but other (nonisotropic) selections are possible. Over-improved stout link smearing, which has been shown to better preserve the topological structure underlying the original configuration, is also employed [33]. The over-improvement parameter ϵ is introduced into the stout link smearing algorithm by modifying the link combinations used in $C_\mu(x)$ such that

$$C^{OI}_\mu(x) = \rho_{\rm sm} \sum \left\{ \frac{5-2\epsilon}{3} (1 \times 1 \text{ staples touching } U_\mu(x)) - \frac{1-\epsilon}{12} (1 \times 2 + 2 \times 1 \text{ staples touching } U_\mu(x)) \right\}$$

and the smearing parameter $\rho_{\rm sm}$ is unchanged.

We then fix the gauge of the smeared links $U^{\rm sm}_\mu$ using the MCG gauge-fixing method. At each iteration of the MCG algorithm we keep track of the total gauge transformation $\Omega^{\rm sm}$ [$\Omega^{\rm sm}(x) \in SU(3)$] that has been applied to $U^{\rm sm}_\mu$. Once the algorithm has converged (to within a tolerance level of 10^{-9}) we use the stored total transformation $\Omega^{\rm sm}$ as a preconditioning gauge transformation for U_μ,

$$U^{\rm pre}_\mu(x) = \Omega^{\rm sm}(x) U_\mu(x) \Omega^{\rm sm\dagger}(x+\mu). \quad (5)$$

We emphasize that the preconditioned field $U^{\rm pre}$ remains on the same gauge orbit as U since the preconditioning is merely a (specific) gauge transformation on the original links. Subsequent gauge fixing of $U^{\rm pre}_\mu$ simply gives us a Gribov copy of the result from gauge fixing U_μ, though the gauge-functional values are expected to be higher than without the preconditioning.

C. The static quark potential

The spectrum of the static quark potential is determined from Wilson loops $W(r,t)$ of area $r \times t$,

$$W(r,t) = \sum_i C_i(r) \exp(-V_i(r) t). \quad (6)$$

In order to enhance $C_1(r)$, which measures the overlap of the loop with the ground state potential, the spatial links are smeared.

Efficient methods exist for the unimproved Wilson action for fine-tuning the smearing parameters to provide optimal overlap with the ground state potential. For $t = 0$, $W(r, t = 0) = 1$ which provides the constraint $\sum_i C_i(r) = 1$ for a given r. For unimproved actions, where the transfer matrix is positive definite, each $C_i(r) \geq 0$. This means $C_1(r)$ can be monitored at large r but small t as the number of smearing sweeps is varied, with the optimal amount of smearing occurring when $C_1(r) \approx 1$. The proximity of $C_1(r)$ to 1 for small t may be easily estimated from the ratio

$$W^{t+1}(r,t)/W^t(r,t+1) \quad (7)$$

which equals $C_1(r)$ in the limit $C_1(r) \to 1$. This provides a quantitative measure of ground-state dominance for unimproved Wilson actions. We note that it is sufficient [37] to fix the smearing fraction α and explore the parameter space via the number of smearing sweeps, n.

This procedure can be repeated for a number of alternate paths of links for a given separation r. By using variational techniques as described in Ref. [38], the combination of paths that gives the greatest overlap with the ground state can be found.

D. Numerical setup

Calculations are performed using 200 quenched configurations with the Lüscher-Weisz plaquette plus rectangle gauge action [39] on a $20^3 \times 40$ lattice with $\beta = 4.52$. The gauge-field parameters are defined by

$$S_G = \frac{5\beta}{3} \sum_{\substack{x\mu\nu \\ \nu>\mu}} \frac{1}{3} \,\mathrm{Re}\,\mathrm{Tr}(1 - P_{\mu\nu}(x)) - \frac{\beta}{12 u_0^2} \sum_{\substack{x\mu\nu \\ \nu>\mu}} \frac{1}{3} \,\mathrm{Re}\,\mathrm{Tr}(2 - R_{\mu\nu}(x)), \quad (8)$$

where $P_{\mu\nu}$ and $R_{\mu\nu}$ are defined in the usual manner and the link product $R_{\mu\nu}$ contains the sum of the rectangular 1×2 and 2×1 Wilson loops. Similar preliminary results have being found on 100 $16^3 \times 32$ lattices (with $\beta = 4.6$) and have been reported elsewhere [40].

Stout link smearing with a smearing parameter of $\rho_{\rm sm} = 0.1$ is used to construct the preconditioning transformation $\Omega^{\rm sm}$ with the number of sweeps ranging from 0 to 20 in steps of four sweeps. We also employ over-improved stout link smearing with a smearing parameter of 0.06 and an ϵ parameter of -0.25.

III. RESULTS

A. The effect of preconditioning

Given that the original goal was to increase the gauge-fixing maxima achieved in MCG fixing, we can see from Table I that we are successful, in this regard, in every case. With each level of preconditioning a higher gauge-functional maximum is achieved both for the smeared gauge field and the preconditioned original field. If we compare zero and four sweeps of preconditioning, we can see that the magnitude of this increase is initially large but the increase is slower as we precondition to higher levels. However, this increase does not come without a cost: the number of gauge-fixing iteration blocks (a block is 50 iterations) required almost doubles between the unpreconditioned fixing and the maximum amount of preconditioning. Typically, two-thirds of the iterations are spent fixing the smeared field and one-third fixing the preconditioned field.

TABLE I. For each of the sweeps used in the preconditioning (OI signifies over-improved stout link smearing), we give the average total number of MCG algorithm iterations used (reported in blocks of 50 iterations with smeared gauge-field iterations summed to preconditioned gauge-field iterations), the average maximum of the gauge functional $V_U[\Omega]$ reached for the smeared links, the average maximum of the gauge functional $V_U[\Omega]$ reached after using the preconditioning transformation, and the percentage of plaquettes that are determined as P vortices after preconditioned gauge fixing.

Sweeps	Iteration blocks	Smear max	Max	Vortices
0	80 ± 20	$\cdots$	0.7350(7)	3.21(12)%
4	118 ± 22	0.9150(11)	0.7400(6)	1.93(10)%
8	126 ± 26	0.9369(54)	0.7407(6)	1.71(10)%
12	126 ± 21	0.9459(12)	0.7411(6)	1.58(10)%
16	128 ± 23	0.9506(12)	0.7412(6)	1.53(10)%
20	135 ± 26	0.9541(12)	0.7414(5)	1.45(11)%
OI 80	148 ± 29	0.9625(14)	0.7417(6)	1.28(13)%

What is most significant about this table, however, is that with each level of preconditioning the percentage of projected plaquettes which are P vortices drops significantly. Without preconditioning 3.21% of plaquettes are vortices, and this drops to as low as 1.28% for the highest level of preconditioning. This is explored in greater detail in the Appendix.

B. The static quark potential

The fact that we can reduce the number of P vortices through preconditioning is not necessarily a cause for concern. Given the center-vortex picture of confinement, our method for determining the location of center vortices is justified only by the relevance of the P vortices that we determine to confinement. A first step in determining this relevance is the calculation of the static quark-antiquark potential. In the center-vortex picture, the string tension σ as determined from the long-range behavior of this potential should be fully accounted for by the center-vortex component of the gauge fields, Z_μ, with the Coulombic term accounted for by the vortex-removed component V_μ. Since we can "remove" the determined P vortices by the operation $U'_\mu(x) = Z^\dagger_\mu(x)U^\Omega_\mu(x)$, we can seek to observe these properties directly. However, since the determined P vortices are gauge dependent (and their number Gribov-copy dependent, as we have already seen), then so too are the subsequent measurements of the static quark potential from the vortex-only, Z_μ, and vortex-removed components, U'_μ, of the configuration.

As described in Sec. II C, the effective potential $V(r)$ is determined from Wilson loops $W(r, t)$ of area $r \times t$. For large t, these loops have the behavior

$$\langle W(r, t)\rangle \propto \exp\{-V(r)t\}.$$

On the lattice, $r := Ra$ and $t := Ta$, where a is the lattice spacing. To obtain the static quark-antiquark potential as a function of the quark separation, we simply repeat the large t (T) fitting procedure of $W(r, t)$ for a range of values of the separation r (R). By using off-axis spatial paths for the Wilson loops, we can obtain noninteger values of R. We exploit full space-time translation to improve the statistics of our Wilson loops.

Since the final representation of $V(r)$ is composed of fits performed on a large number of effective potential plots for all the different separations R, it is prudent and necessary that the factors determining those fits are given, and taken into account, when analyzing the subsequent static quark-antiquark potential as a function of separation. The difficulties associated with such fits can be easily recognized in Figs. 1 and 2. In these plots we show the effective potential for a variety of quark separations for each of the original (Fig. 1), vortex-only, and vortex-removed configurations (Fig. 2). On the left side of Fig. 2 we show these plots for the MCG fixing without preconditioning, while on the right we show the same plots with 80 sweeps of over-improved smearing as a preconditioner.

One of the first things to discuss is the difficulty in obtaining a satisfactory fit range for the data, particularly in the case of the vortex-removed configurations. With these configurations, and more so at larger separations, the potential falls rapidly and decays into noise quickly. A visually satisfying plateau region is not evident and we must rely on the fitting routine to determine the goodness of the fit. What the plot can tell us is that the effective potential continues to fall (at separations of five lattice spacings and greater) until, at least, the time slice $T = 5$. Since the data decay into noise around this point, we chose to constrain our fit using time slice 5 and fit from this slice to slice 7 (a straightline fit to three points). This constraint is then applied to all values of the separation. What we find

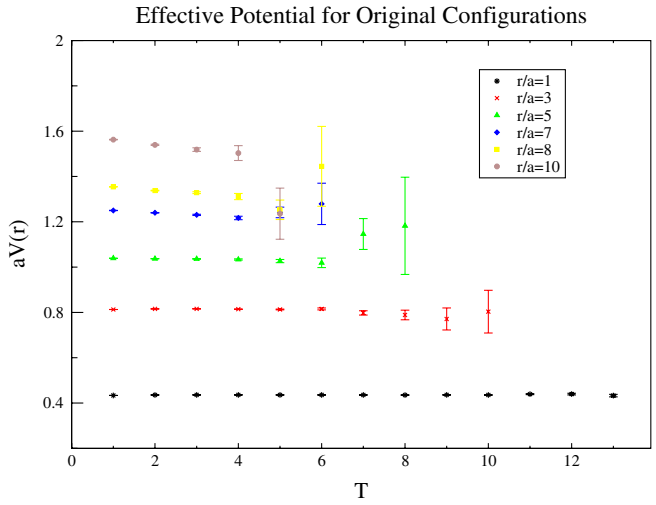

FIG. 1 (color online). The effective potential for the original configurations for a range of quark separations.

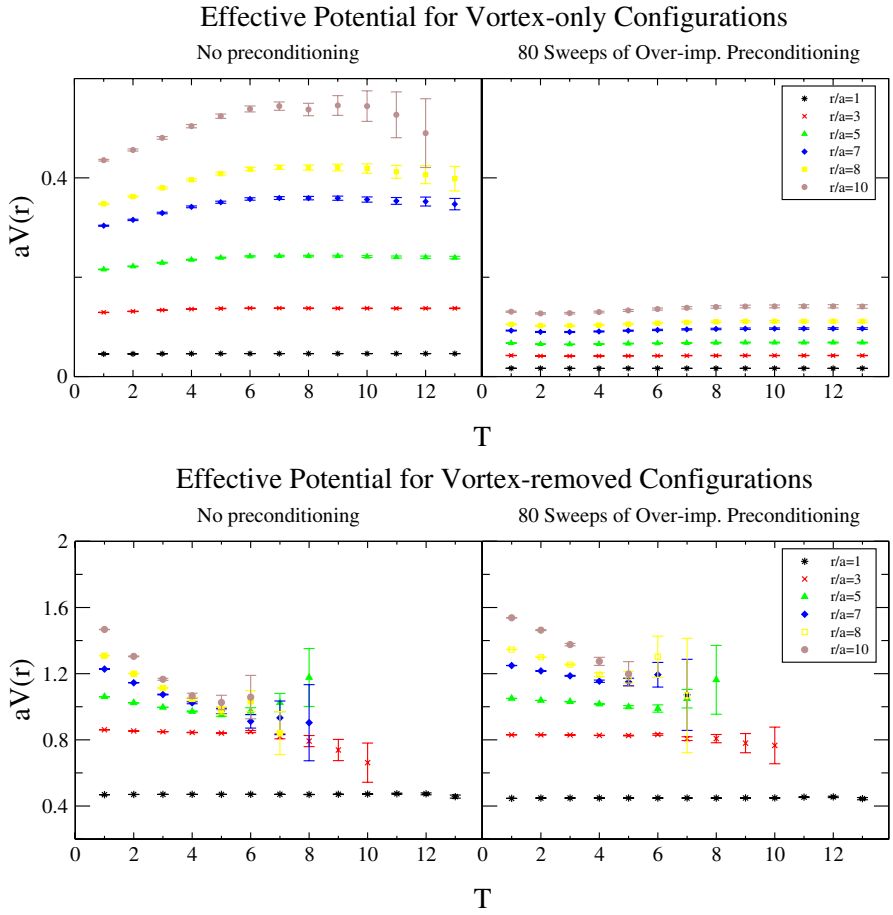

FIG. 2 (color online). The effective potential plots for the MCG-fixed configurations without preconditioning (left panels) and with the highest level of preconditioning (right panels). The upper plots contain the data for the vortex-only configurations, and the lower for the vortex-removed configurations. Each plot contains data for a range of quark separations.

is that, while this may lead to reasonable ($\lesssim 1.3$) values of the χ^2 per degree of freedom in the majority of cases, there are certainly significant deviations from this desirable result.

Global fit ranges are chosen in a somewhat similar way for the original (Fig. 1) and vortex-only configurations (upper graphs of Fig. 2). For the original configurations, the global fit range was chosen to be between time slice 4 and 6 since these accounted for the systematic drift of the potential at large separations for lower time values and also gave reasonable χ^2 behavior. In the case of the vortex-only configurations, the errors are far more controlled, but the potential rises at small times and plateaus far later; therefore, the fit range was chosen to be from time slice 10 to 12, but again some of the χ^2 per degree of freedom values were unsatisfactory. This is most likely due to the heavy constraints placed on the fit by the accurate potential determinations.

Of significant concern when comparing the potentials of the unpreconditioned and preconditioned results in Figs. 1 and 2 is the direct comparison of the potentials in each case. Figure 1 shows the potential after gauge fixing but prior to the center projection and vortex removal. When comparing the preconditioned data to the unpreconditioned data in Fig. 2, we can see that the rate of decay for the preconditioned data has fallen significantly. Given the resolution of this data for larger values of T, it is not possible to verify whether the plateaus from both cases coincide for all quark separations. Of course the most dramatic effect occurs for the vortex-only data of Fig. 2. There is a dramatic reduction in the magnitude of potential for all separations, and this is a direct manifestation of the Gribov-copy effect for this gauge-fixing method.

This Gribov-copy effect is also manifest in Fig. 3. Here we show plots of the static quark potential as a function of separation for three of the six levels of preconditioning used, as well as the unpreconditioned data. It would appear that the findings are consistent with loss of confinement upon P-vortex removal. Although it would seem that this is perhaps not such a reasonable observation in the over-improved case, if we look exclusively at the on-axis contributions to the potential in this case (Fig. 4) and compare

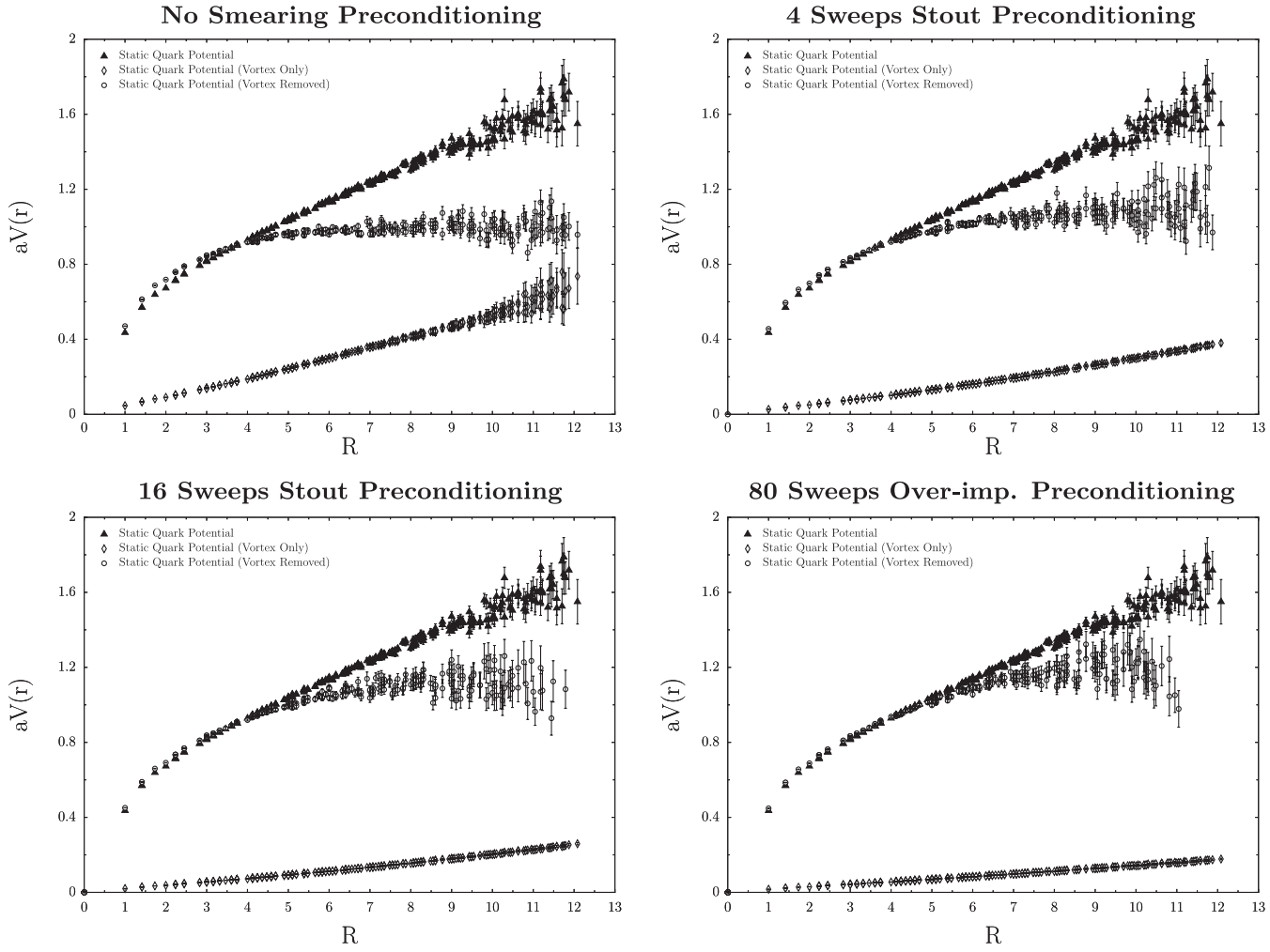

FIG. 3. Static quark-antiquark potential plots for each of the preconditioning smearing sweeps used. Each plot contains data for the full, vortex-removed, and vortex-only configurations. The data shown use a three time-slice fit window in each case, with the fit window being from time slice 4 to 6 for the full data, time slice 5 to 7 for the vortex-removed data, and time slice 10 to 12 for the vortex-only data.

it to that of the unpreconditioned case, we observe that the potential does approach an asymptote, but only at larger values of the separation. This would concur with our previous observation that the potential takes longer to plateau in this case, and therefore the fit window may not be adequately accounting for this effect. Careful examination of the vortex-removed results also reveals that we obtain an increasingly more accurate fit to the short-range Coulombic portion of the potential with higher preconditioning levels.

If we fit the potential to the ansatz,

$$V(r) = V_0 + \sigma r - \frac{\alpha}{r}, \tag{9}$$

where σ is called the string tension, what is more significant is that the value of the string tension determined from the vortex-only configurations drops dramatically, and systematically, from $\sim$60% to as low as $\sim$16% of the full string tension ($\sigma = 0.05441$, as determined from the static quark potential on the original configurations) with increased preconditioning. This is a disturbing manifestation of the Gribov problem since it perhaps questions how accurately we have determined the center vortices by our projection of the P vortices with our fixing method.

C. Discussion

The use of smearing as a preconditioning technique does indeed lead to higher maxima in the MCG gauge-fixing condition $V_U[\Omega]$. These higher maxima in turn lead to lower numbers of P vortices determined in the center projection. In $SU(2)$, similar results have been obtained when seeking higher maxima by means of simulated annealing [26] and by prefixing to Landau gauge prior to MCG fixing [25]. As observed in $SU(2)$ [26,27], there appears to be a significant anticorrelation between the

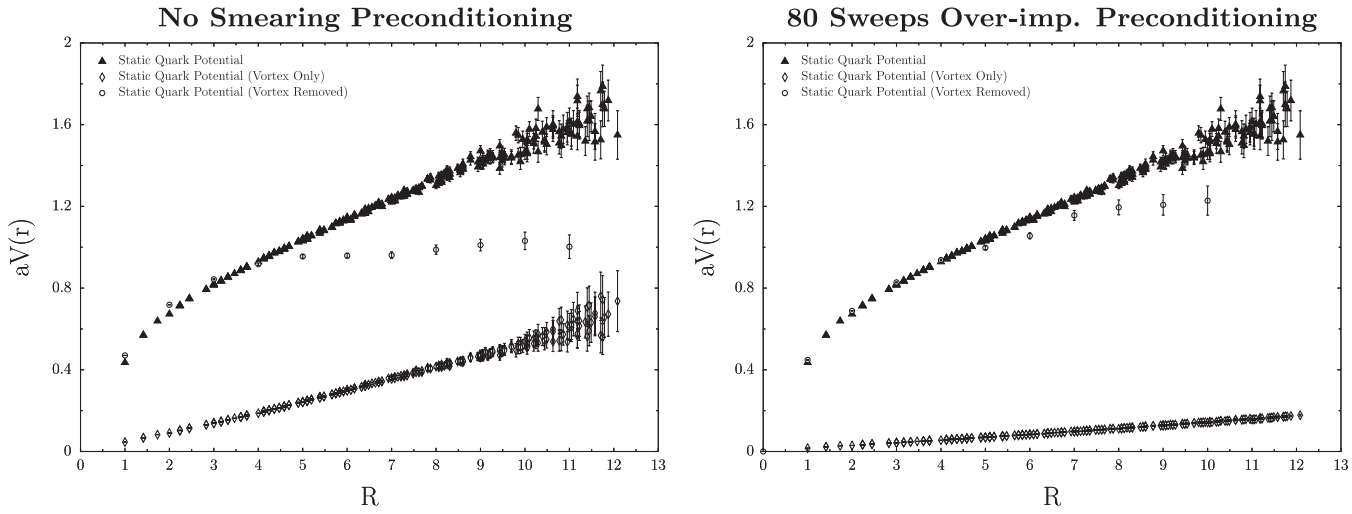

FIG. 4. The static quark-antiquark potential plots for both the lowest (left panel) and highest (right panel) levels of preconditioning. Only the on-axis data are shown for the vortex-removed configurations.

value achieved in the gauge-fixing functional and the percentage of the full string tension reproduced by center vortices.

As can be seen in Fig. 5, the ratio between the vortex-only string tension σ and the vortex density ρ_{vortices} (defined as the fraction of P-vortex plaquettes to the total number of plaquettes) as a function of preconditioning is not independent of the preconditioning. Had this ratio been constant, one could conclude that the reduction in the string tension is simply associated with not identifying all the center vortices present in the configuration. Either the mechanism with which vortices produce confinement is not entirely intact or the physical relevance of the P vortices is not uniformly distributed, rendering the density measure ineffective.

In $SU(2)$, it was seen that smearing an $SU(2)$ configuration prior to MCG fixing reduced the center-projected string tension considerably [4]. It was argued in Ref. [4] that this reduction is due to smearing greatly expanding the vortex cores making the MCG process of compressing them (such that they pierce a single plaquette) more difficult. A similar point was used to address the issue raised by prefixing to Landau gauge [25]. In principle, the same position could be taken here; the generated preconditioning transformation may allow the vortex cores to be distributed across a larger number of lattice sites and again make the MCG task of compressing them more difficult. However, the over-improved stout link smearing parameters are deliberately chosen to maintain the size of instantons, and there is a case to say that if the link between center vortices and topology seen in $SU(2)$ persists in $SU(3)$, then it should be possible to smear configurations without expanding the vortex cores. It is difficult to attribute the same vortex-expanding behavior to the case of simulated annealing. However, the fact that known higher maxima exist (having these properties) and that simulated annealing is designed to locate them could explain the similar behavior.

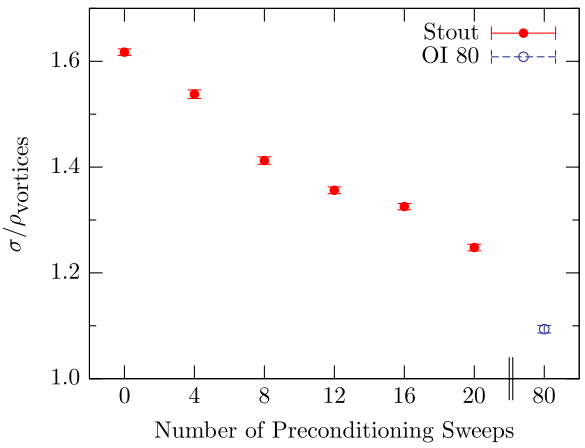

FIG. 5 (color online). Ratio between the vortex-only string tension and the vortex density as a function of preconditioning.

It is significant that much of the discussion in Ref. [15], where there is no Gribov ambiguity, can also be reconciled with the results found here. In this case a number of different Laplacian operators were constructed simply by using smeared links in the definition of the operator. There, too, it was seen that this caused an analogous effect on the vortex-only string tension. It was argued that the use of smearing caused the Laplacian to be blind to the short-range physics, making the decomposition of the gauge field into the confining and nonconfining components less effective—disorder in the vortex-only component is absorbed into the vortex-removed component resulting in a loss of string tension. It was contended there that in the continuum limit the smearing radius shrinks to zero, restoring the string tension.

In the same way, the smearing preconditioning may allow this effect to occur for MCG. That the locations of

TABLE II. Comparisons between different preconditioning levels of stout link smearing (OI signifies over-improved stout link smearing). In the upper-right triangle of this table (from preconditioning level row to preconditioning level column) we report the percentage of configurations that experience a reduction in the measured number of P vortices. The lower-left triangle (preconditioning level column to preconditioning level row) of this table gives the percentage reduction of the number of P vortices (for the configurations that experienced a reduction).

Sweeps	0	4	8	12	16	20	OI 80
0	⋱	100	100	100	100	100	100
4	$39^{\pm 4}$	⋱	96.5	100	100	100	100
8	$46^{\pm 4}$	$11^{\pm 6}$	⋱	81.5	91.5	97.5	99.5
12	$50^{\pm 4}$	$17^{\pm 6}$	$9^{\pm 6}$	⋱	69	81	97.5
16	$52^{\pm 3}$	$20^{\pm 6}$	$12^{\pm 6}$	$7^{\pm 5}$	⋱	69.5	95.5
20	$54^{\pm 4}$	$24^{\pm 7}$	$15^{\pm 7}$	$10^{\pm 7}$	$8^{\pm 6}$	⋱	85.5
OI 80	$59^{\pm 4}$	$33^{\pm 7}$	$24^{\pm 8}$	$19^{\pm 9}$	$16^{\pm 9}$	$14^{\pm 8}$	⋱

vortices as determined by MCG and the gauge defects of the Laplacian method coincide serves to strengthen this position [15]. Indeed, as discussed in Ref. [15], periodic boundary conditions cause gauge defects to have an opposite partner and, perhaps, the nonlocality introduced by the preconditioning procedure may allow these opposites to annihilate, producing no net defect after projection and a resultant drop in the vortex-only string tension.

IV. CONCLUSIONS

It is found that the use of smearing as a preconditioning technique leads to higher maxima in the MCG gauge-fixing functional $V_U[\Omega]$. The achieved higher maxima in turn lead to lower numbers of P vortices determined in the center projection and, subsequently, lower values of the vortex-only string tension.

Although the fundamental modular region of MCG would be an ideal candidate for a unique definition of vortex texture, it seems that the vortex matter arising from the first Gribov region of MCG as a whole has greater phenomenological relevance. While all preconditionings lead to a loss of string tension, it is the center-projected physics that is not consistent. An improvement in $V_U[\Omega]$ causes one to miss vortices in the projection and spoil the phenomenology.

While MCG has proven successful to a large extent in $SU(2)$, what is different in $SU(3)$ is that center projection has never been shown to find enough vortices to reproduce the full string tension.[1] Indeed, improving the maximum achieved by the gauge-fixing functional leads to fewer vortices and poor phenomenology. It would be informative to look for correlations between the locations of the determined P vortices with each preconditioning since their removal still leads to a loss of string tension.

[1]Apart from possibly vortices as determined via Laplacian gauge [15] in the continuum limit.

The key discovery of this paper is one of anticorrelation—the higher the MCG gauge-fixing functional, the worse the phenomenology picture.

ACKNOWLEDGMENTS

We thank the Australian Partnership for Advanced Computing (APAC) and eResearch South Australia for generous grants of supercomputer time which have enabled this project. We also thank the University of Adelaide Faculty of Sciences for providing time on their Condor™ cycle-scavenging system. This work is supported by the Australian Research Council.

APPENDIX: THE EFFECT OF PRECONDITIONING ON THE NUMBER OF P VORTICES

In Table II we investigate further the reduction in the measured number of P vortices when using preconditioned gauge fixing by looking in detail at this particular effect between all the different levels of preconditioning. The table is divided into upper-right and lower-left triangles. In the upper triangle we report the percentage of configurations that experience a reduction in the measured number of P vortices when the number of smearing sweeps used in the preconditioning is increased. As we can see, this percentage is always high but the effect is lessened as we move to transitions, particularly small transitions, between the higher levels of preconditioning. It should be noted, however, that the relative difference between, for example, 20 sweeps of stout link and 80 sweeps of over-improved stout link preconditioning is difficult to quantify (given the difference in algorithms) but the effect is still significant for this transition.

The magnitude of this reduction in P vortices determined is also reported in Table II. When reading from

TABLE III. Comparisons between different preconditioning levels of stout link smearing (OI signifies over-improved stout link smearing). When reading from sweep row to sweep column (upper-right triangle) the value shown is the percentage of configurations that achieve a higher maximum of the gauge-fixing functional. When reading from sweep column to sweep row (lower-left triangle) the value shown is the percentage of the configurations with a higher maximum that also achieve a lower number of P vortices determined.

Sweeps	0	4	8	12	16	20	OI 80
0	⋱	100	100	100	100	100	100
4	100	⋱	89.5	98	99	100	100
8	100	100	⋱	75	78.5	89.5	93.5
12	100	100	95.33	⋱	59	71.5	87.5
16	100	100	98.09	97.46	⋱	62.5	77.5
20	100	100	100	97.2	93.6	⋱	71
OI 80	100	100	100	100	100	97.18	⋱

the lower-left triangle (preconditioning level column to preconditioning level row) of this table, we can see the reduction (in %) of the number of P vortices reported for the configurations that experienced a reduction. In the transition from no preconditioning to any other level, the order of a 50% reduction is observed. For other transitions it would seem the effect drops to the 10% level reasonably quickly, but again we see an increased effect when we consider over-improved smearing. It should be noted that, regardless of the preconditioning level, the center phases of the links of the fields always remain evenly distributed across the three possible values, reflecting the fact that the realization of center symmetry remains unaffected.

We refer to Table III when considering whether a higher maximum of the gauge-fixing functional translates into a lower number of P vortices. When reading from preconditioning sweep row to preconditioning sweep column (upper-right triangle), the percentage of configurations that experience an increase in the gauge-fixing maximum is shown. Similar trends to that of Table II are observed, with large effects initially, which become reduced for small transitions between higher levels of preconditioning. Of these configurations with an increased maximum, we can see almost exclusively (when reading from preconditioning level column to preconditioning level row in the lower-left triangle) that an increased gauge-fixing maximum does lead to a lower number of P vortices being determined.

[1] R. Alkofer and J. Greensite, J. Phys. G **34**, S3 (2007).
[2] J. Greensite, Prog. Part. Nucl. Phys. **51**, 1 (2003).
[3] A. S. Kronfeld, M. L. Laursen, G. Schierholz, and U. J. Wiese, Phys. Lett. B **198**, 516 (1987).
[4] L. Del Debbio, M. Faber, J. Giedt, J. Greensite, and S. Olejnik, Phys. Rev. D **58**, 094501 (1998).
[5] G. S. Bali, V. Bornyakov, M. Müller-Preussker, and K. Schilling, Phys. Rev. D **54**, 2863 (1996).
[6] R. Bertle, M. Faber, J. Greensite, and S. Olejnik, Nucl. Phys. B, Proc. Suppl. **94**, 482 (2001).
[7] O. Miyamura, Phys. Lett. B **353**, 91 (1995).
[8] S. Sasaki and O. Miyamura, Phys. Rev. D **59**, 094507 (1999).
[9] V. G. Bornyakov, E. M. Ilgenfritz, B. V. Martemyanov, S. M. Morozov, M. Müller-Preussker, and A. I. Veselov, Phys. Rev. D **77**, 074507 (2008).
[10] P. de Forcrand and M. D'Elia, Phys. Rev. Lett. **82**, 4582 (1999).
[11] C. Alexandrou, M. D'Elia, and P. de Forcrand, Nucl. Phys. B, Proc. Suppl. **83**, 437 (2000).
[12] J. Gattnar, C. Gattringer, K. Langfeld, H. Reinhardt, A. Schafer, S. Solbrig, and T. Tok, Nucl. Phys. **B716**, 105 (2005).
[13] F. V. Gubarev, S. M. Morozov, M. I. Polikarpov, and V. I. Zakharov, Pis'ma Zh. Eksp. Teor. Fiz. **82**, 381 (2005) [JETP Lett. **82**, 343 (2005)].
[14] P. O. Bowman, K. Langfeld, D. B. Leinweber, A. O' Cais, A. Sternbeck, L. von Smekal, and A. G. Williams, Phys. Rev. D **78**, 054509 (2008); P. O. Bowman *et al.*, Proc. Sci., CONFINEMENT8 (2008) 056.
[15] P. de Forcrand and M. Pepe, Nucl. Phys. **B598**, 557 (2001).
[16] J. Ambjorn, J. Giedt, and J. Greensite, J. High Energy Phys. 02 (2000) 033.
[17] A. V. Kovalenko, M. I. Polikarpov, S. N. Syritsyn, and V. I. Zakharov, Phys. Rev. D **71**, 054511 (2005).
[18] P. Y. Boyko *et al.*, Nucl. Phys. **B756**, 71 (2006).
[19] A. Montero, Phys. Lett. B **467**, 106 (1999).
[20] M. Faber, J. Greensite, and S. Olejnik, Phys. Lett. B **474**, 177 (2000).
[21] K. Langfeld, Phys. Rev. D **69**, 014503 (2004).

[22] D. B. Leinweber, P. O. Bowman, U. M. Heller, D. J. Kusterer, K. Langfeld, and A. G. Williams, Nucl. Phys. B, Proc. Suppl. **161**, 130 (2006).
[23] J. D. Stack, W. W. Tucker, and R. J. Wensley, Nucl. Phys. **B639**, 203 (2002).
[24] V. G. Bornyakov *et al.* (DIK Collaboration), Phys. Rev. D **70**, 074511 (2004).
[25] T. G. Kovacs and E. T. Tomboulis, Phys. Lett. B **463**, 104 (1999).
[26] V. G. Bornyakov, D. A. Komarov, and M. I. Polikarpov, Phys. Lett. B **497**, 151 (2001).
[27] M. Faber, J. Greensite, and S. Olejnik, Phys. Rev. D **64**, 034511 (2001).
[28] C. Alexandrou, P. de Forcrand, and M. D'Elia, Nucl. Phys. **A663**, 1031c (2000).
[29] K. Langfeld, H. Reinhardt, and O. Tennert, Phys. Lett. B **419**, 317 (1998).
[30] K. Langfeld, H. Reinhardt, and A. Schafke, Phys. Lett. B **504**, 338 (2001).
[31] J. E. Hetrick and Ph. de Forcrand, Nucl. Phys. B, Proc. Suppl. **63**, 838 (1998).
[32] C. Morningstar and M. J. Peardon, Phys. Rev. D **69**, 054501 (2004).
[33] P. J. Moran and D. B. Leinweber, Phys. Rev. D **77**, 094501 (2008).
[34] E. M. Ilgenfritz, D. Leinweber, P. Moran, K. Koller, G. Schierholz, and V. Weinberg, Phys. Rev. D **77**, 074502 (2008); **77**, 099902(E) (2008).
[35] M. Faber, J. Greensite, and S. Olejnik, J. High Energy Phys. 01 (1999) 008.
[36] M. Faber, J. Greensite, S. Olejnik, and D. Yamada, Nucl. Phys. B, Proc. Suppl. **83**, 527 (2000).
[37] F. D. Bonnet, P. Fitzhenry, D. B. Leinweber, M. R. Stanford, and A. G. Williams, Phys. Rev. D **62**, 094509 (2000).
[38] C. J. Morningstar and M. J. Peardon, Phys. Rev. D **56**, 4043 (1997).
[39] M. Lüscher and P. Weisz, Commun. Math. Phys. **97**, 59 (1985); **98**, 433(E) (1985).
[40] A. O. Cais, W. Kamleh, B. Lasscock, D. Leinweber, L. von Smekal, and K. Langfeld, Proc. Sci., LAT2007 (2007) 321.